



# Experimental study on the pseudo threshold pressure gradient of supported fractures in shale reservoirs

Jidong Gao<sup>1</sup> · Weiyao Zhu<sup>1</sup> · Aishan Li<sup>2</sup> · Yuexiang He<sup>1</sup> · Liaoyuan Zhang<sup>2</sup> · Debin Kong<sup>1</sup>

Received: 21 April 2022 / Accepted: 13 March 2024  
© The Author(s) 2024

## Abstract

Pseudo threshold pressure gradient (PTPG) exists in the propped fractured reservoir, but its nonlinear flow law remains unclear. The effects of the mineral composition of shale and microstructure of fracturing fluid on PTPG were analyzed by X-ray diffraction and liquid nitrogen quick-freezing method. The results demonstrate that a proppant with a large particle size is more likely to form an effective flow channel and reduce liquid flow resistance, thus decreasing PTPG and increasing conductivity. The polymer fracturing fluid with rectangular microstructures significantly increased the PTPG supporting the fractured core. Experimental results show that the PTPG of the resin-coated sand-supported core in the fracturing fluid with a concentration of 1.2% is 245 times higher than that in the fracturing fluid with a concentration of 0.1% when the confining pressure is 5 MPa. Wetting hysteresis and the Jamin effect are responsible for the rise of PTPG in two-phase flow. The equivalent fracture width shows a good power function relationship with the PTPG. Thus, this study further explains the nonlinear flow behavior of reservoirs with fully propped fractures.

**Keywords** Pseudo threshold pressure gradient · Proppant · Shale reservoir · Equivalent fracture width · Residual fracturing fluid

## List of symbols

$A$	Cross-section area of the core fracture (cm <sup>2</sup> )
$A_p$	Proppant cross-sectional area (mm <sup>2</sup> )
$a$	Coefficients of the equivalent fracture width
$b$	Coefficients of the equivalent fracture width
$D_f$	Fracture conductivity (μm <sup>2</sup> cm)
$d_f$	Splitting section width (cm)
$K$	Core permeability (D)
$L$	Major axis length of proppant (mm)
$p_c$	Capillary force (Pa)
$Q$	Flow rate of the fluid through the porous medium (mL/s)
$r$	Capillary radius (m)
$S$	Proppant sphericity
$w_f$	Equivalent fracture width (cm)
$\theta_1$	Advancing contact angle (°)

$\theta_2$	Receding contact angle (°)
$\lambda$	PTPG (MPa/m)
$\sigma$	Two-phase interfacial tension (N/m)
$\nabla p$	Pressure gradient (MPa/m)
$\mu$	Fluid viscosity (mPa s)

## Introduction

Shale contains large amounts of dense clay minerals and nano-scale pores with high heterogeneity and much lower permeability than dense sandstones and carbonates (Muther et al. 2021; Syed et al. 2022). Horizontal well fracturing technology is currently the core method for shale oil and gas production. This fracturing technology can expand the contact area of reservoir fractures, thus enhancing the oil recovery rate (Hou et al. 2018; Ostad-Ali-Askari et al. 2019; Liew et al. 2020; Zhang et al. 2020; Shen et al. 2021). Due to the low permeability of shale oil reservoirs, a large threshold pressure gradient still exists even under large-scale hydraulic fracturing, resulting in shale oil production cannot be guaranteed (Katende et al. 2021a, b). The addition of proppant to the reservoir fracture system through fracturing fluid can effectively prolong fracture closure time and improve

✉ Debin Kong  
Kongdb@ustb.edu.cn

<sup>1</sup> School of Civil and Resources Engineering, University of Science and Technology Beijing, Beijing 100083, China

<sup>2</sup> Petroleum Engineering Technology Research Institute, Sinopec Shengli Oilfield Company, Dongying 257000, Shandong, China

fracture conductivity, thereby bringing more economic benefits to increase oil/gas production (Wu et al. 2018, 2021; Golian et al. 2020; Chun et al. 2020, 2021).

Pseudo threshold pressure gradient (PTPG) is the intersection of the reverse extension of the straight-line portion of the "pressure gradient-flow curve" in low-velocity non-Darcy flow and the x-coordinate (Dong et al. 2019; Zhu et al. 2022). With the increase of the PTPG, crude oil presents a nonlinear flow trend in the formation, which significantly impacts the productivity of low-permeability tight oil reservoirs (Liu 2020; Zhao et al. 2020a, b; Liu et al. 2020a, b). Many scholars have studied the nonlinear seepage of low-permeability reservoir matrix systems. Based on the capillary model, a fractal model considering the threshold pressure gradient was established for low permeability tight reservoirs; it can well reflect the influence of microscopic pore structures on the threshold pressure (Ye et al. 2019). Xiao et al. (2021a, b) conducted a series of PTPG experiments on nano-scale channels and cores. Their results demonstrated that there was a pressure threshold when liquid flowed through nano-channels and cores. The fluid properties and pore diameter can affect the threshold pressure of the micro-nano channel. Thus, the functional expressions of permeability, water saturation, effective stress, and PTPG were fitted through high-precision experiments since the threshold pressure gradient is an important factor affecting the control zone. Additionally, the experimental model was finally applied to the dynamic well pattern (Dong et al. 2019; Wang et al. 2019).

There are many types of proppants, among which quartz sand, nutshells, and glass beads are the conventional ones. Resin-coated sand and ceramics are advanced proppants. The cost of advanced proppants is much higher than that of conventional proppants. In contrast, advanced proppants also have better compression resistance (Melcher et al. 2020). The fluid viscosity and proppant type, strength, particle size, sphericity, circularity and density are all important factors affecting fracture conductivity (Katende et al. 2021b). Many scholars have conducted targeted studies on the above-mentioned influencing factors. By filling the fractures with quartz sand and ceramics proppant in different proportions, fracture conductivity was tested to judge the influence of the proppant type on it. Results showed high fracture conductivity of the ceramics proppant with high roundness, with three times the flow capacity of quartz sand. When the quartz sand is subjected to higher confining pressure, it is more likely to become fine debris to block the flow channel and reduce the conductivity of fractures (Liang et al. 2020). The size of the proppant also affects the conductivity. Proppants with large particle sizes usually lead to better fracture conductivity; accordingly, they have greater contact area and pressure with the fracture and are more likely to break into small fragments blocking the flow channel (Bandara

et al. 2021). The stress sensitivity of proppant embedment, proppant fracture conductivity, permeability, and surrounding pressure are correlated. Some scholars have confirmed that proppant fracture conductivity is a function of proppant particle size, filling porosity, and surrounding pressure (Benge et al. 2021; Katende et al. 2022). Proppant embedment is a significant cause of the decrease in fracture width and conductivity (Voltolini and Ajo-Franklin 2020; Zhi and Elsworth 2020). Both embedment and transport of the proppant reduce the transport capacity of propped fractures. Proppants with small particle sizes are easier to transport (Zhang et al. 2022). Experiments and numerical simulation studies have shown that proppant embedment is related to the plastic strength of the proppant. Since the proppant is in contact with the oil shale, the local shale undergoes shear deformation when the formation pressure increases, embedding the proppant into the rock (Katende et al. 2021b; Ahamed et al. 2022). Based on the fracture width model of the shale reservoir, the random filling of the proppant in the fracture was simulated in a discrete element model according to the mechanical properties of the proppant and reservoir. The effect of proppant deformation on fracture width and conductivity during pressure closure was analyzed, and the relationship between fracture width and conductivity was predicted (Jiang et al. 2020; Xu et al. 2021). A finite element model with a rough cross-section was established using 3D scanning of real fractured rock slabs. The results showed that the embedment depth of the proppant was positively correlated with the closure stress and proppant elastic modulus (Zhao et al. 2022).

However, the proppant placement is usually in a single layer or non-uniform sparse in actual propped fractured reservoirs. Although the conductivity of fractures can be improved locally, an obvious threshold pressure gradient still exists in the propped fracture reservoir (Chuprakov et al. 2021; Xiao et al. 2021a, b). There is still no consistent conclusion on the influencing factors and changing laws of its nonlinear flow (Ni, et al 2018; Zheng et al. 2019; Wu et al. 2019). Additionally, there are still no relevant reports on the in-depth analysis of factors affecting the PTPG of fully propped through-fractured shale cores by experimental methods and the relationship between the equivalent fracture width of fully propped fractures and the PTPG.

In this study, factors affecting the PTPG variation in propped fractures were fully analyzed to investigate the mechanism of PTPG variation. A series of single-phase and two-phase flow experiments in propped fractures were conducted using displacement fluids with different viscosities and proppant types. Furthermore, the effect of fracturing fluid was analyzed by scanning electron microscope (SEM) using the liquid nitrogen quick-freezing method. Then, the equivalent fracture width and PTPG were fitted nonlinearly based on experimental data. This study can provide a

**Table 1** Analysis of shale mineral composition

Mineral composition	Clay	Quartz	Potassium feldspar	Calcite	Plagioclase	Dolomite	Pyrite	Analcite	Barite
Content %	23.4	8.7	0.4	51.1	1.0	11.3	3.6	0.2	0.3

**Table 2** Salinity of formation water

Salinity	NaCl	Na <sub>2</sub> SO <sub>4</sub>	NaHCO <sub>3</sub>	CaCl <sub>2</sub>	MgCl <sub>2</sub> · 6H <sub>2</sub> O
Content g/L	2.92	0.11	0.04	0.89	0.21

reference for researchers to understand and predict the non-linear flow laws in fully propped fractured reservoirs.

## Experiments and methods

### Experimental materials

In the experiment, natural cores were extracted from the ultra-low permeability shale reservoir at a depth of 3447 m in Shengli Oilfield, China. The core is 2.5 cm in diameter and 5.1 cm in length. The porosity is 4.534%, and the original gas permeability is  $0.0106 \times 10^{-3} \mu\text{m}^2$ . The mineral composition of shale was analyzed using X-ray diffraction. Table 1 shows the mineral composition of shale cores. Calcite, clay, dolomite, and quartz have the highest proportions. Calcite, dolomite, and quartz are brittle minerals. In addition, the average pore size of the core is on the nanometer scale.

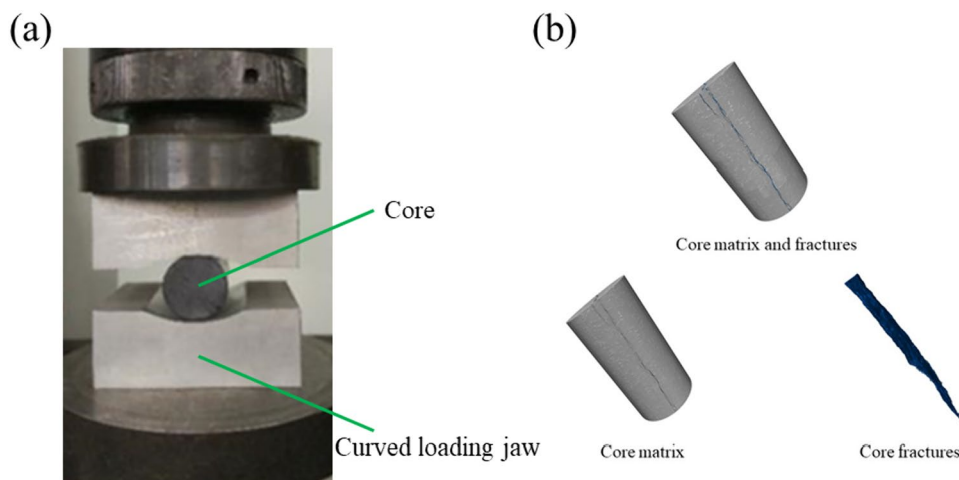
Quartz sand with 40–60 mesh, 60–100 mesh, and 100–200 mesh at a bulk density of 1.22 g/mL, resin-coated sand with 40–60 mesh at a bulk density of 1.40 g/mL, and ceramicsite with 40–60 mesh at a bulk density of 1.46 g/mL were used as the experimental proppants. Silicone oil with a shear viscosity of 3.00 mPa s was adopted. The water used

in this study was prepared indoors according to the parameters of formation water in Shengli Oilfield. Table 2 shows that the proportion of NaCl per liter of formation water is the highest, and the proportion of NaHCO<sub>3</sub> is the lowest. Formation water and polyacrylamide (PAM) polymer were mixed in different proportions to prepare fracturing fluids with different viscosities. The formation water from Shengli Oilfield was used to configure PAM as a low-viscosity fracturing fluid with a mass concentration of 0.1% and a shear viscosity of 5.90 mPa s and a high-viscosity fracturing fluid with a mass concentration of 1.2% and a shear viscosity of 40.17 mPa s.

### Experimental apparatus

The real core was split along the symmetry axis of the bedding plane using the Brazilian splitting method, and its surface roughness can be used to simulate hydraulic fracturing, as shown in Fig. 1a. Then, the core was wrapped with tetrachloroethylene tape and placed in the center of a curved loading clamp made of soft aluminum, with a loading speed of 0.05 mm/min. The experiment was stopped when the load dropped. Subsequently, fractures were extracted from the core matrix using a micro-CT scanner (NanoVoxel-3502E) and a threshold segmentation method (Fig. 1b). The total fracture volume of the core is  $0.207 \text{ cm}^3$ , and the average fracture width is  $1.62 \times 10^{-2} \text{ cm}$ . The specific surface area of the fracture, which is the fracture area per unit fracture volume, is  $1.522 \times 10^{-2} \text{ m}^2/\text{g}$ . The smaller the specific surface area, the better the connectivity across the fractured core.

**Fig. 1** a Brazilian splitting method for core preparation, b CT scan core



Finally, a certain mass of proppant was weighed, evenly placed on the split section of the core and sealed with tetrachloroethylene tape and two filter papers to prepare a fully supported through-fracture core.

As shown in Fig. 2, the equipment consists of a displacement control module, a confining pressure control module, and a data acquisition module. Among them, the displacement control module comprises a high-precision ISCO double-cylinder pump, three switches, and three intermediate containers, which can effectively control the pumping speed of different experimental fluids. The confining pressure control module consists of a hand pump, a pressure gauge, and a core holder. This module can precisely control the confining pressure of the fully supported through-fracture core. The data acquisition module includes a differential pressure sensor and a computer. This module can transmit the pressure difference at both ends of the core holder to the computer in the form of data through the differential pressure sensor to realize real-time monitoring and recording of the differential pressure. Furthermore, the microstructure of fracturing fluids was photographed using Regulus 8100 SEM.

## Experimental procedures

The PTPG of the prepared fully supported through-fracture cores at different viscosities of silicone oil, fracturing fluid, and residual fracturing fluid was tested experimentally. The specific implementation steps are as follows:

### (1) Core preparation

The Brazilian splitting method was used for loading and splitting along the centerline of the bedding direction of the columnar core at a loading speed of 0.05 mm/min. Then, the splitting section length of the core was measured after drying in an oven at 105°C for more than 24 h. Finally, a certain mass of proppant was weighed, evenly placed on the split section of the core and sealed with tetrachloroethylene tape and two filter papers to prepare a fully supported through-fracture core.

### (2) Vacuum saturation

The core was placed in a core holder, and a vacuum pump was connected to the end of the core holder and pumped for 82 h to reduce experimental error. Subsequently, a double-cylinder pump was turned on to

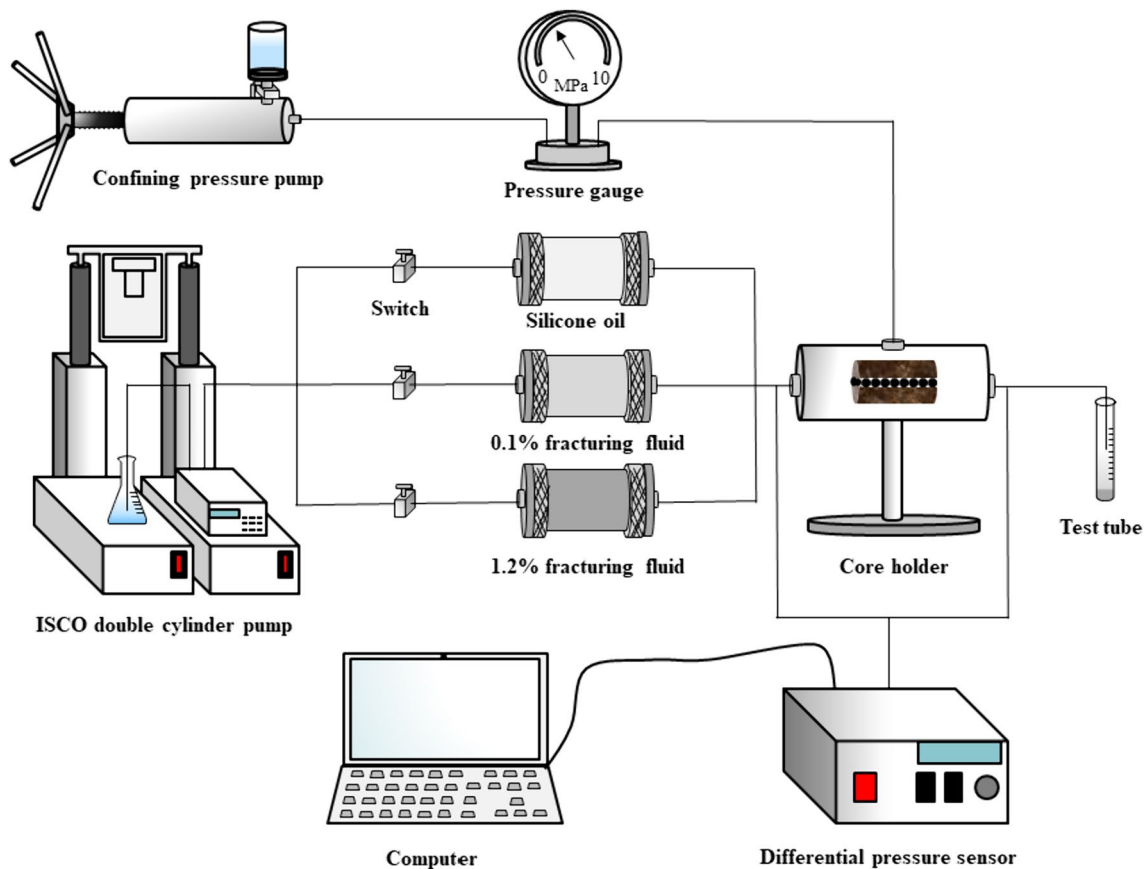


Fig. 2 Experimental apparatus

saturate the experimental fluid at a constant flow rate of 0.04 mL/min. The core was fully saturated with fluid when the single-phase fluid flowed steadily out of the core holder outlet.

(3) Liquid displacement

After the liquid was placed in the intermediate container, the high-precision double-cylinder pump was used for displacement. Experiments were conducted under different confining pressure conditions (3 MPa, 5 MPa, and 7 MPa). The fluid in the intermediate container flowed through the fully supported penetration core at a constant repulsion flow rate, and the flow rate was measured for at least 1 h. Experimental data were recorded after the differential pressure was stabilized by observing the differential pressure sensor. Subsequently, the above operation was repeated after changing the displacement velocity of the liquid. There were at least five sets of displacement velocities at the same confining pressure.

(4) Data processing

The pressure gradient and flow rate obtained from experiments at different confining pressures were plotted as the "pressure gradient-flow rate" relationship curve and linearly regressed to the x-coordinate. The intersection of the curve and the x-coordinate was the PTPG of the fully supported through-fracture core.

(5) Image acquisition

Images of the fracture core, fracturing fluid, and proppant were acquired using a high-precision microscope and SEM. A high-precision microscope was used to observe the proppant and core. SEM equipment combined with the rapid nitrogen freezing method was used to observe the microscopic images of the fracturing fluid.

## Results and discussion

In the experiment, the PTPG of fully supported fracture cores was tested using the controlled variable method by varying the proppant particle size, proppant type, and fluid viscosity. The specific experimental schemes are shown in Table 3. Cases 1–3 show the effect of the mesh number of proppants on the PTPG of fracture. Cases 4–9 show the effects of quartz sand, resin-coated sand, and ceramsite on the PTPG of fracture under two different viscosity fracturing fluids. In case 10, 1.2% fracturing fluid was saturated into the propped fracture core, and silicone oil was used as displacement fluid to study the effects of two-phase flow on the PTPG of fracture.

### Influence of particle sizes of proppant on the PTPG

Figure 3 shows the PTPG of three different particle sizes (40–60 mesh, 60–100 mesh, and 100–200 mesh) of quartz sand proppants on the fully propped fracture core at a placement concentration of 0.5 kg/m<sup>2</sup> and a fracture conductivity of 5 MPa. Silicone oil with a viscosity of 3 mPa·s was selected as the experimental fluid in cases 1–3.

The results show that the PTPG of 100–200 mesh quartz sand is the largest, and it changes in the range of  $5 \times 10^{-4}$ – $8 \times 10^{-4}$  MPa/m when the confining pressure increases from 3 to 7 MPa. The PTPG of 60–100 mesh quartz sand proppant is lower than that of 100–200 mesh quartz sand, and it varies in the range of  $1 \times 10^{-4}$ – $5 \times 10^{-4}$  MPa/m. However, the average PTPG of 40–60 mesh quartz sand proppant is  $5 \times 10^{-5}$  MPa/m. It can be concluded that the PTPG is approximately 0 when the particle size of the selected quartz sand proppant is greater than 0.3 mm. The cores used in this experiment are fractured cores composed of large particle size proppant

**Table 3** Experimental schemes

Case	Proppant	Mesh	Sphericity	Placement concentration (kg/m <sup>2</sup> )	Bulk density (g/mL)	Fluid	Viscosity (mPa s)	Saturated fluid
1	Quartz sand	40–60	0.591	0.5	1.22	Silicone oil	3.00	Silicone oil
2	Quartz sand	60–100	0.591	0.5	1.22	Silicone oil	3.00	Silicone oil
3	Quartz sand	100–200	0.591	0.5	1.22	Silicone oil	3.00	Silicone oil
4	Quartz sand	40–60	0.591	0.5	1.22	0.1% fracture fluid	5.90	0.1% fracture fluid
5	Resin-coated sand	40–60	0.668	0.5	1.40	0.1% fracture fluid	5.90	0.1% fracture fluid
6	Ceramsite	40–60	0.858	0.5	1.46	0.1% fracture fluid	5.90	0.1% fracture fluid
7	Quartz sand	40–60	0.591	0.5	1.22	1.2% fracture fluid	40.17	1.2% fracture fluid
8	Resin-coated sand	40–60	0.668	0.5	1.40	1.2% fracture fluid	40.17	1.2% fracture fluid
9	Ceramsite	40–60	0.858	0.5	1.46	1.2% fracture fluid	40.17	1.2% fracture fluid
10	Quartz sand	40–60	0.591	0.5	1.22	Silicone oil	3.00	1.2% fracture fluid

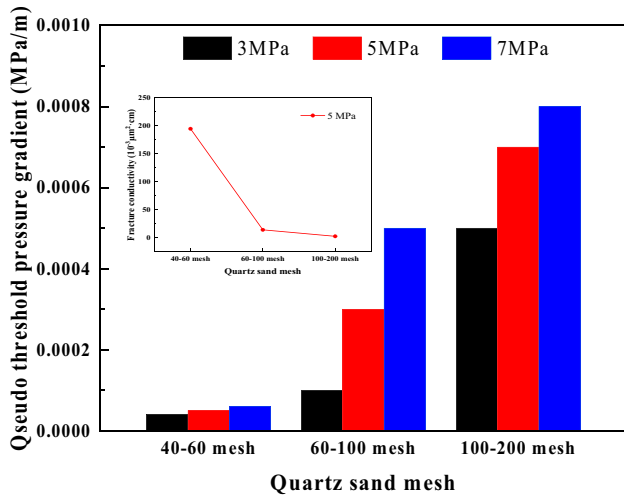


Fig. 3 PTPG and fracture conductivity of the quartz sand mesh-silicon oil system

with high average porosity and loose proppant arrangement, which is easy to form dominant flow channels (Xu et al. 2019). The fluid flow resistance in this flow channel decreases, which is expressed macroscopically as a reduction in PTPG (Li et al. 2022). Therefore, the PTPG of the fully propped fractured core decreases with the increase of the proppant particle sizes.

Furthermore, the PTPG increases to varying degrees when the confining pressure increases (Liu et al. 2021a, b), which can be attributed to the properties of shale cores and proppants. The brittleness index is the proportion of calcite, quartz, potassium feldspar, and plagioclase in rock minerals. Table 1 shows that the brittleness index of the Shengli shale core used in this experiment is 61.2%. As shown in Fig. 4, the shale matrix will be partially trapped in the proppant when the confining pressure increases, thus decreasing the fracture width and effective flow path area (Katende et al. 2021a). Additionally, the increasing confining pressure will also cause the proppant to break into smaller particles, resulting in increased PTPG of fractures (Chen et al. 2017; Ahamed et al. 2021b).

The conductivity of the fully propped fracture core is related to the PTPG. Increasing the conductivity of the fracture will reduce the PTPG of the fracture (Kong et al. 2022b). The accompanying figure in Fig. 3 shows the fracture conductivity at 5 MPa for three different proppant mesh sizes. The maximum fracture conductivity of 40–60 mesh quartz sand is  $194.86 \times 10^{-3} \mu\text{m}^2 \text{cm}$ , and its corresponding PTPG is  $5 \times 10^{-5} \text{MPa/m}$ . The minimum fracture conductivity of 100–200 mesh quartz sand is  $2.44 \times 10^{-3} \mu\text{m}^2 \text{cm}$ , and its corresponding PTPG is  $7 \times 10^{-4} \text{MPa/m}$ .

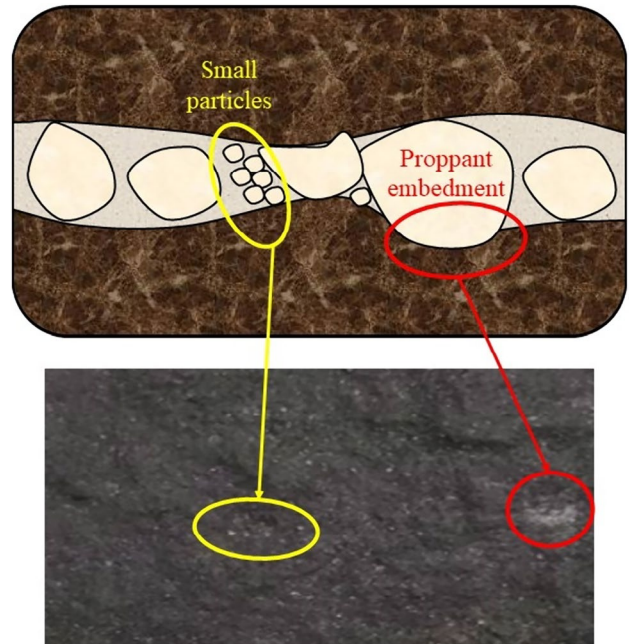


Fig. 4 Proppant breakage and embedment

### Influence of proppant types and fracturing fluid combinations on the PTPG

In this section, the placement concentration is  $0.5 \text{ kg/m}^2$ . Additionally, 40–60 mesh quartz sand, resin-coated sand, and ceramicsite were used as proppants. A low-viscosity fracturing fluid with a shear viscosity of  $5.90 \text{ mPa}\cdot\text{s}$  and a high-viscosity fracturing fluid with a shear viscosity of  $40.17 \text{ mPa}\cdot\text{s}$  were used as experimental fluids in cases 4–9. The experimental results are shown in Fig. 5. The variation law of the three proppants in the fracturing fluid with a concentration of 0.1% is shown in Fig. 5a. Their variation law in the fracturing fluid with a concentration of 1.2% is shown in Fig. 5b. The PTPG of the cores prepared from quartz sand, resin-coated sand, and ceramicsite in fracturing fluid gradually decreases, which is because the sphericity of different proppants is different. Sphericity is defined as a dimensionless number with values ranging from 0 to 1. As sphericity approaches 1, the surface of the proppant becomes smoother and more spherical. As sphericity approaches 0, the proppant surface is rougher and more irregular. The pore volume of high sphericity proppants also increases. The sphericity can be calculated by Eq. (1) (Zheng et al. 2018).

$$S = \frac{4A_p}{\pi L^2} \quad (1)$$

where  $S$  is the sphericity of the proppant;  $A_p$  is the cross-section area ( $\text{mm}^2$ );  $L$  is the major axis length (mm).

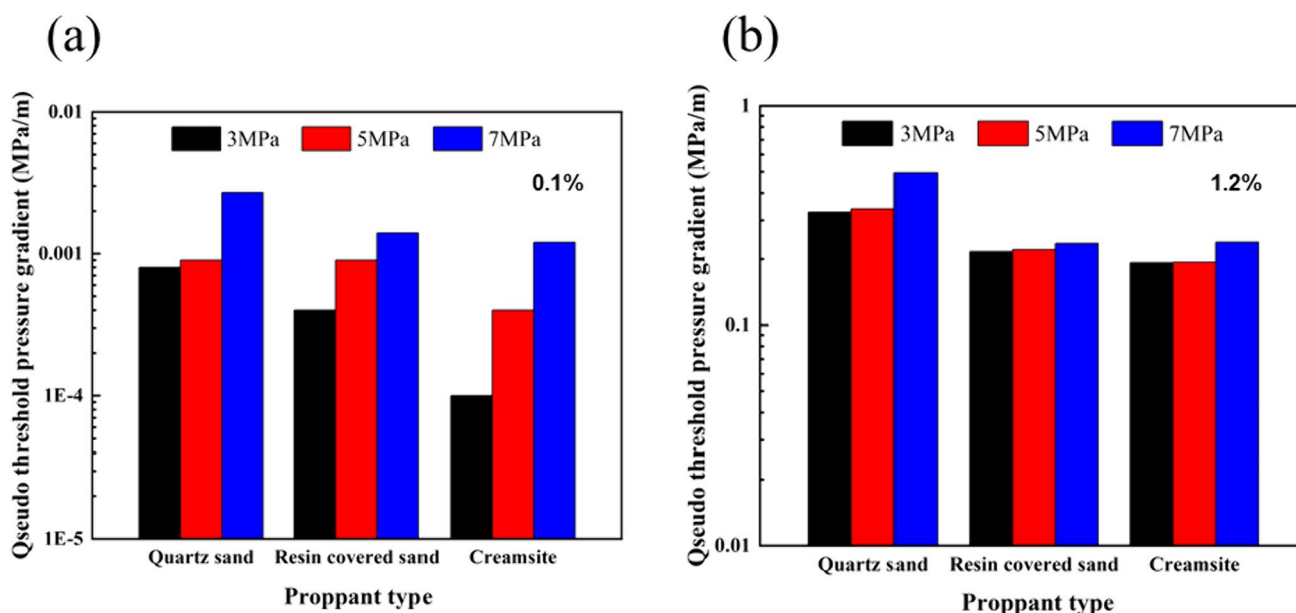


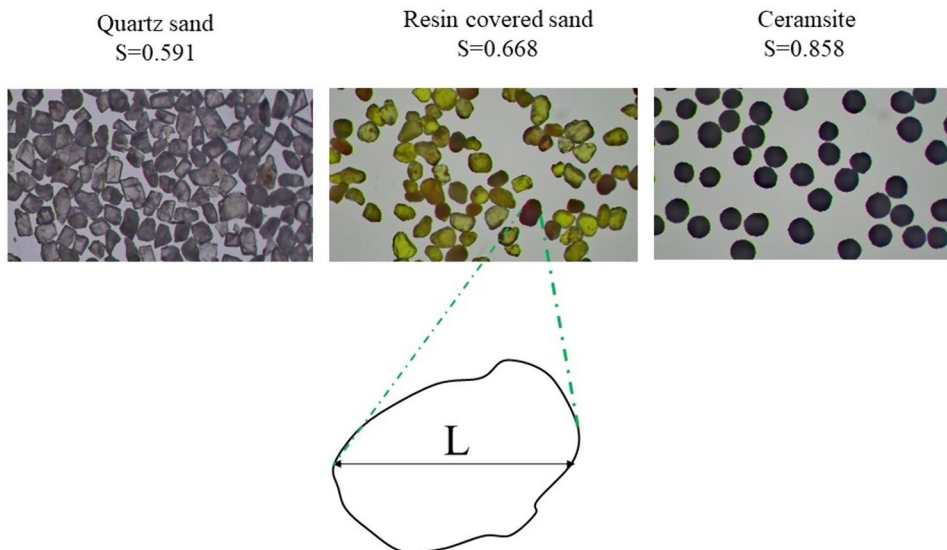
Fig. 5 a PTPG of proppant types (0.1% fracturing fluid), b PTPG of proppant types (1.2% fracturing fluid)

Then, the major axis lengths and areas of the three proppants were measured using a high-precision microscope, and their values were calculated by Eq. (1) to obtain the sphericity. The calculation results are shown in Fig. 6. The sphericity of quartz sand, ceramsite, and resin-coated sand are 0.591, 0.858, and 0.668, respectively. The ceramsite proppant has the highest sphericity, and the effective flow channel of the porous medium composed of ceramsite is also the largest. Therefore, the PTPG of the fully propped-through fracture cores is also the smallest (Qiao et al. 2022).

As shown in Fig. 5a, b, the viscosity of fracturing fluid greatly influences the PTPG of fully supported fractured

cores. Taking resin-coated sand as an example, the PTPG of the cores under the two viscosity fracturing fluids differs by 245 times when the confining pressure is 5 MPa. When the viscosity of the fracturing fluid increases, the high viscosity of the fracturing fluid will block the effective flow channels between proppants and increase the PTPG (You et al. 2019). The PTPG of the cores in the high-viscosity fracturing fluid varies little with the confining pressure, which can be explained by the microstructure of the fracturing fluid. The SEM image of the microstructure of the fracturing fluid is shown in Fig. 7. The SEM and the liquid nitrogen quick-freezing method were used to rapidly solidify and

Fig. 6 The sphericity of different proppants



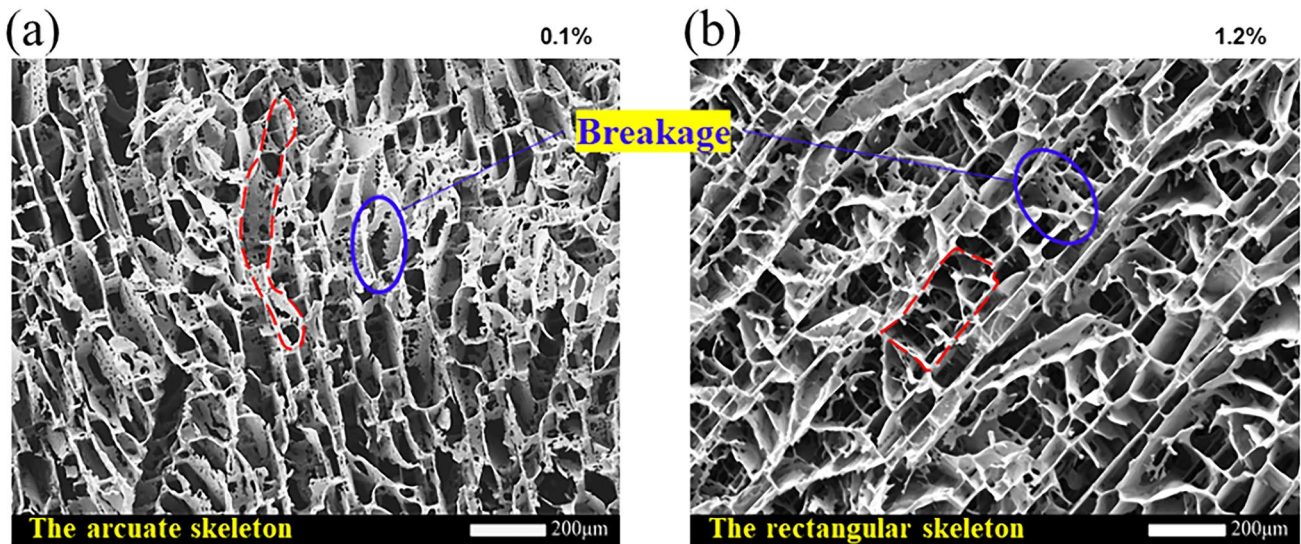


Fig. 7 a SEM of 0.1% fracturing fluid microstructure, b SEM of 1.2% fracturing fluid microstructure

sublime the water molecules in the fracturing fluid solution, thereby obtaining the original microstructure of the fracturing fluid. The fracturing fluids comprise polymers with a network skeleton structure, which can effectively absorb water molecules and increase flow resistance (Kong et al. 2019). Compared with acid gel fracturing fluid, its structure is more orderly and three-dimensional, but the connections between the main polymerization chains are more sparse (Zhao et al. 2020a, b).

The comparison of the blue areas between Fig. 7a, b shows that low-viscosity fracturing fluid is more prone to undergo extensive damage under shear stress. The fracturing fluid with this structure has an unstable ability to absorb water molecules and poor structural stability. The comparison of the red areas between Fig. 7a, b suggests that the high-viscosity fracturing fluid has a rectangular skeleton structure and is not fully stretched, and the ductility and deformability of the structure are stronger. In addition, the high-viscosity fracturing fluid has a rectangular skeleton structure, which is more stable and can withstand stronger tensile forces. The stability of the fracturing fluid with this structure will be further increased after combining with water molecules, and the viscosity will be more significant. Therefore, increasing the confining pressure to a small range will not lead to a sharp rise in the PTPG.

### Influence of residual fracturing fluid on the PTPG

It is necessary to address the current problems of reservoir damage, decreased fracture conductivity, and increased PTPG caused by using fracturing fluids in shale reservoirs (Liu et al. 2020a, b). In this section, 40–60 mesh quartz sand proppant was used to prepare cores and saturate 1.2%

fracturing fluid. Silicone oil was used as the displacement fluid. The PTPG of silicone oil was tested with residual fracturing fluids in case 10. The experimental results are shown in Fig. 8. The PTPG of silicone oil is 0.0138, 0.0237, and 0.0244 MPa/m at confining pressures of 3, 5, and 7 MPa, respectively. However, the PTPG of the silicone oil in the fractured core is approximately 0 when silicone oil is used as the saturated fluid and displacement fluid. The two experiments show that the residual fracturing fluid can cause the PTPG to rise rapidly in the fully propped fractured core and damage the fracture conductivity (You et al. 2019).

Taking 5 MPa as an example, the fracture conductivity under the residual fracturing fluid-silicone oil

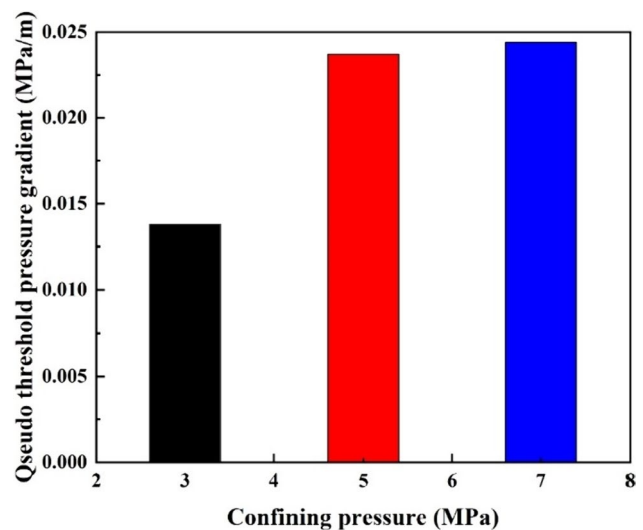


Fig. 8 PTPG of the residual fracturing fluid-silicone oil system



system and silicone oil single-phase flow is  $6.22 \times 10^{-3}$  and  $194.86 \times 10^{-3} \mu\text{m}^2\cdot\text{cm}$ , respectively, a difference of 31 times. The reason is related to proppant fractures and shale matrix parts.

In the porous medium composed of quartz sand fractures, the high viscosity of fracturing fluid will block its effective flow channels, resulting in an extremely rapid rise of the PTPG (Huang et al. 2020). Furthermore, the pore throat difference is further widened, and heterogeneity is strengthened after the porous medium is blocked by the fracturing fluid. In two-phase seepage, the additional resistance effect is called the Jamin effect when the droplet passes through the pore throat (Liu et al. 2021a, b). When oil droplets pass through different pores, the Jamin effect occurs, increasing the resistance to oil displacement, which is macroscopically manifested as an increase in PTPG.

The porosity of the shale matrix is much smaller than that of the porous medium composed of quartz sand. Therefore, the shale matrix has a thick boundary layer fluid (Dong et al. 2019). Additionally, there is a wetting hysteresis in the two-phase flow. It is difficult to form a continuous oil-phase fluid in the two-phase flow. The oil phase in the capillary can be cut off by the fracturing fluid to form discontinuous oil droplets due to the complex capillary network of the shale matrix (Fig. 9). When the capillary force  $p_c=0$ , the oil droplet is stationary in the capillary. When the capillary force  $p_c>0$ , the silicone oil-fracturing fluid interface in the capillary is deformed,  $\theta_1>\theta_0>\theta_2$ . At this time, the pressure difference in the capillary force on both sides of the fracturing fluid is uneven, and the resultant force is opposite to the displacement force, thus

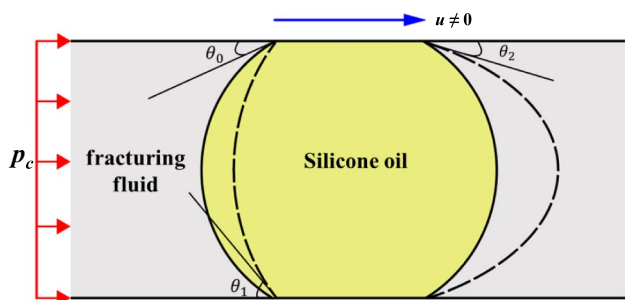
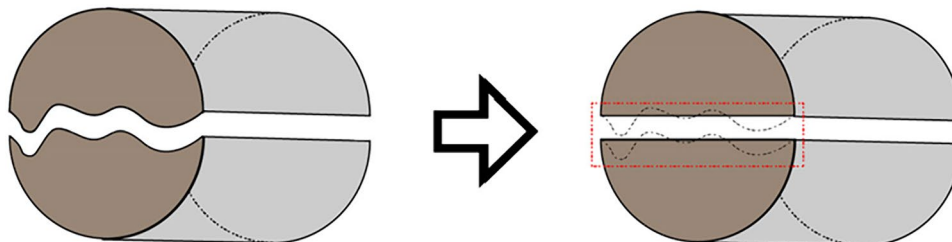


Fig. 9 Wetting hysteresis in the two-phase flow

Fig. 10 Equivalent fracture width



forming the PTPG. The capillary force can be calculated by Eq. (2) (Gao et al. 2021; Kong et al. 2022b).

$$p_c = \frac{2\sigma}{r} (\cos \theta_2 - \cos \theta_1) \tag{2}$$

where  $p_c$  is capillary force (Pa);  $\sigma$  is two-phase interfacial tension (N/m);  $r$  is the capillary radius (m);  $\theta_1$  and  $\theta_2$  are advancing and receding contact angles ( $^\circ$ ), respectively.

For the shale matrix with nano-scale pores, the additional resistance caused by the wetting hysteresis will be larger, thus increasing the PTPG (Huang et al. 2021).

### Influence of equivalent fracture width on the PTPG

To further study the relationship between fracture width and PTPG, the following principle is used to calculate the equivalent fracture width between fractures. First, Eq. (3) (Gao et al. 2020; Han et al. 2018) is used to test the permeability of fully supported through-fracture cores:

$$K = \frac{Q\mu}{10A(\Delta p - \lambda)} \tag{3}$$

where  $Q$  is the flow rate of the fluid through the porous medium (mL/s);  $A$  is the cross-sectional area of fracture ( $\text{cm}^2$ );  $K$  is permeability ( $\mu\text{m}^2$ );  $\Delta p$  is the pressure gradient (MPa/m);  $\mu$  is fluid viscosity (mPa-s);  $\lambda$  is PTPG (MPa/m).

The cleavage section of the core is shown in Fig. 1b. The overall cleavage section is rectangular but has a rough section. The original gas-measured permeability of the columnar shale core is  $0.0106 \times 10^{-3} \mu\text{m}^2$ , and the fully supported fractured core is  $8254.10 \times 10^{-3} \mu\text{m}^2$ . The permeability of the shale matrix is reduced by 5 orders of magnitude compared with the porous media composed of proppant. The shale matrix has a low contribution rate to the permeability of fully supported through-fracture cores. Thus, rough-split sections can be equivalent to smooth sections parallel to each other. As shown in Fig. 10, its flow can be expressed as Eq. (4) (Ahamed et al. 2021a):

$$Q = \frac{10d_f w_f^3 (\Delta p - \lambda)}{12\mu} \tag{4}$$

where  $d_f$  is the splitting section width (cm), and  $W_f$  is the equivalent fracture width (cm).

The conductivity of a fracture is defined as the product of the permeability of the fluid flowing through the porous medium and the equivalent fracture width. After the simplification of the model in Fig. 10, the conductivity of the fracture can be expressed as Eq. (5):

$$D_f = \frac{Q\mu}{10d_f(\Delta p - \lambda)} \quad (5)$$

where  $D_f$  is conductivity ( $\mu\text{m}^2\cdot\text{cm}$ ).

Substituting Eq. (4) into Eq. (3) can obtain the relationship between the permeability and the equivalent fracture width. After substituting the result into Eq. (5), the relationship between the equivalent fracture width and conductivity can be obtained, as shown in Eq. (6):

$$w_f = \sqrt[3]{12D_f} \quad (6)$$

The equivalent fracture width of cases 4–6 was calculated using the above principle. The experimental results were fitted to obtain the relationship between the fracture width and the PTPG. The results are shown in Fig. 11 and Table 4. The variation curve of the PTPG with equivalent fracture width in 0.1% concentration fracturing fluid is shown in Fig. 11a. The variation curve of the PTPG with equivalent fracture width in 1.2% concentration fracturing fluid is shown in Fig. 11b. Table 4 shows that the maximum correlation coefficient between equivalent fracture width and PTPG in the two fracturing fluids is 0.908. The equivalent fracture width of the fully propped fractured core in two viscosity fracturing fluids has a good power function relationship with

**Table 4** Fitting parameters of equivalent fracture width and PTPG in different solutions

Fluid	Formulation	Correlation coefficient ( $R^2$ )
0.1% fracture fluid	$\lambda = 5.01 \times 10^{-12} w_f^{-4.74}$	0.90775
1.2% fracture fluid	$\lambda = 2.91 \times 10^{-8} w_f^{-3.45}$	0.83158

the PTPG. The expressions of the PTPG and the equivalent fracture width are shown in Eq. (7).

$$\lambda = a w_f^b \quad (7)$$

where  $a$  and  $b$  are the coefficients of the equivalent fracture width.

The fitting results show that viscosity is the main influencing parameter of  $a$  and  $b$ . The viscosity  $\mu$  is positively correlated with  $a$ . When the viscosity increases, the parameter and PTPG also show an increasing trend, which is consistent with the experimental law. Similarly, viscosity has an important influence on  $b$ . When the viscosity increases,  $b$  tends to  $-1$ , and the PTPG changes relatively flat. The effects of confining pressure and proppant sphericity on the equivalent fracture width of the fracture decrease as viscosity increases. In addition, the effect of sphericity  $S$  on parameter  $a$  was studied. The results are shown in the subplot of Fig. 11a. Furthermore, data were fitted for three different proppants. The parameter fluctuates in the range

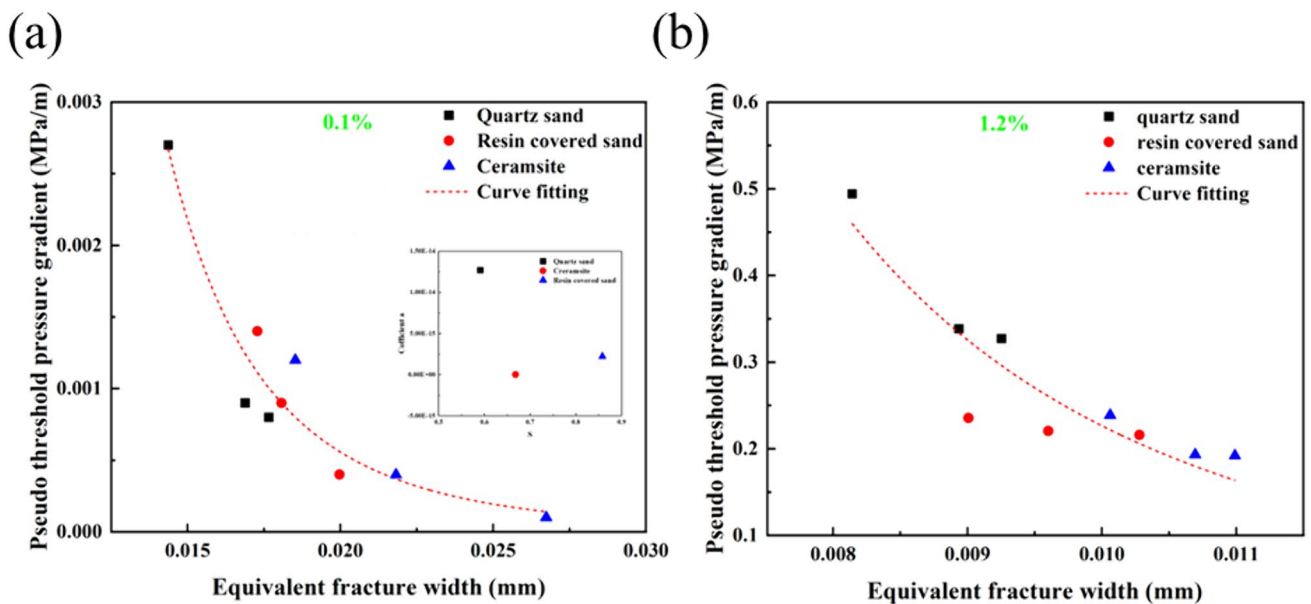


**Fig. 11** **a** Variation curve of PTPG with equivalent fracture width in 0.1% concentration fracturing fluid; **b** Variation curve of PTPG with equivalent fracture width in 1.2% concentration fracturing fluid

of  $1.01 \times 10^{-18}$ – $1.27 \times 10^{-14}$  with a small range of variation. Therefore, the sphericity  $S$  has little influence on parameter  $a$ .

In summary, the larger the equivalent fracture width of the fracture, the larger the effective flow path and the smaller the PTPG. The higher the sphericity of the proppant, the larger the equivalent fracture width and the smaller the PTPG. The smaller the confining pressure and fluid viscosity, the larger the equivalent fracture width, and the smaller the PTPG (Huang et al. 2021).

## Conclusions

The effects of proppant type, fracture, embedment, fluid viscosity, and fracture width on supported fracture pseudo threshold pressure gradient (PTPG) were studied under controlled laboratory conditions. Conclusions are drawn as follows:

- (1) The larger the particle size of the proppant, the lower the confining pressure, and the smaller the PTPG of supporting fracture cores. The PTPG of fracture is negatively correlated with the flow conductivity. Proppant with large particle size is more likely to form an effective flow channel under low confining pressure, and the liquid flow resistance is reduced, which is manifested as lower PTPG and increased conductivity.
- (2) The polymer fracturing fluid with rectangular microstructure significantly increases the PTPG of supporting the fractured core. The experimental results show that at a confining pressure of 5 MPa, the PTPG of a core supported by resin-coated sand in a fracturing fluid with a concentration of 1.2% is 245 times higher than that in a fracturing fluid with a concentration of 0.1%.
- (3) Residual fracturing fluid can increase the heterogeneity of the pores of the propped fractured core, thus damaging the fracture conductivity. In this study, the residual fracturing fluid reduces the fracture conductivity by 31 times. Wetting hysteresis and the Jamin effect are the main factors leading to the rise of PTPG in two-phase flow, and wetting hysteresis cannot be ignored in nano-scale pores.
- (4) The equivalent fracture width has a good power function relationship with the PTPG. The maximum correlation coefficient is 0.908. The viscosity is the main factor for the equivalent fracture width parameters  $a$  and  $b$ . The larger the equivalent fracture width, the smaller the PTPG. The effect of confining pressure and proppant sphericity on the equivalent fracture width of the fracture decreases as viscosity increases.

**Funding** The authors acknowledge the financial support from the Natural Sciences Foundation of China (No. 42102163) and the Fundamental Research Funds of the Central Universities (No. FRF-TP-20-006A1).

## Declarations

**Competing Interest** The authors declare that they have no known competing financial interests or personal relationships that could have appeared to influence the work reported in this paper.

**Ethical statements** We confirm that this work is original and has not been published elsewhere, nor is it currently under consideration for publication elsewhere.

**Open Access** This article is licensed under a Creative Commons Attribution 4.0 International License, which permits use, sharing, adaptation, distribution and reproduction in any medium or format, as long as you give appropriate credit to the original author(s) and the source, provide a link to the Creative Commons licence, and indicate if changes were made. The images or other third party material in this article are included in the article's Creative Commons licence, unless indicated otherwise in a credit line to the material. If material is not included in the article's Creative Commons licence and your intended use is not permitted by statutory regulation or exceeds the permitted use, you will need to obtain permission directly from the copyright holder. To view a copy of this licence, visit <http://creativecommons.org/licenses/by/4.0/>.

## References

- Ahamed M, Perera M, Elsworth D et al (2021a) Effective application of proppants during the hydraulic fracturing of coal seam gas reservoirs: Implications from laboratory testings of propped and unpropped coal fractures. *Fuel* 304:121394
- Ahamed MAA, Perera MSA, Black JR et al (2021b) Investigating the proppant damage mechanisms expected in a propped coal fracture and its effect on fracture flow. *J Petrol Sci Eng* 198:108170
- Ahamed M, Perera M, Ranjith P (2022) Implementation of an elastoplastic constitutive model to study the proppant embedment in coal under different pore fluid saturation conditions: a numerical and experimental study. *Fuel* 317:123488
- Bandara K, Ranjith P, Rathnaweera T et al (2021) Crushing and embedment of proppant packs under cyclic loading: An insight to enhanced unconventional oil/gas recovery. *Geosci Front* 12(6):100970
- Benge M, Lu Y, Katende A, et al. (2021) Connecting Geomechanical properties with potential for proppant embedment and production decline for the emerging Caney Shale. URTEC-2021-5084-MS, Oklahoma. In: SPE/AAPG/SEG Unconventional Resources Technology Conference
- Chen D, Ye Z, Pan Z et al (2017) A permeability model for the hydraulic fracture filled with proppant packs under the combined effect of compaction and embedment. *J Pet Sci Eng* 149:428–435
- Chun T, Li Y, Wu K (2020) Comprehensive experimental study of proppant transport in an inclined fracture. *J Petrol Sci Eng* 184:106523
- Chun T, Zhu D, Zhang Z, et al. (2021) Experimental study of proppant transport in complex fractures with horizontal bedding planes for slickwater fracturing. SPE-199877-PA SPE Production Operations 36(01):83–96

- Chuprakov D, Iuldasheva A, Alekseev A (2021) Criterion of proppant pack mobilization by filtrating fluids: theory and experiments. *J Pet Sci Eng* 196:107792
- Dong M, Yue X, Shi X et al (2019) Effect of dynamic pseudo threshold pressure gradient on well production performance in low-permeability and tight oil reservoirs. *J Pet Sci Eng* 173:69–76
- Gao Y, Lin Q, Bijeljic B, Blunt MJ (2020) Pore-scale dynamics and the multiphase Darcy law. *Phys Rev Fluids* 5(1):013801
- Gao Y, Wu K, Chen Z et al (2021) Effect of wetting hysteresis on fluid flow in shale oil reservoirs. *Energy Fuels* 35:12075–12082
- Golian M, Katibeh H, Singh VP et al (2020) Prediction of tunnelling impact on flow rates of adjacent extraction water wells. *Q J Eng GeolHydrogeol* 53(2):236–251
- Han G, Liu Y, Nawnt K et al (2018) Discussion on seepage governing equations for low permeability reservoirs with a threshold pressure gradient. *Adv Geo-Energy Res* 2(3):245–259
- Hou B, Zhang R, Zeng Y et al (2018) Analysis of hydraulic fracture initiation and propagation in deep shale formation with high horizontal stress difference. *J Pet Sci Eng* 170:231–243
- Huang F, Dong C, Shang X, You Z (2021) Effects of proppant wettability and size on transport and retention of coal fines in saturated proppant packs: experimental and theoretical studies. *Energy Fuels* 35(15):11976–11991
- Huang Q, Liu S, Cheng W, Wang G (2020) Fracture permeability damage and recovery behaviors with fracturing fluid treatment of coal: an experimental study. *Fuel* 282:118809
- Jiang S, Chen P, Yan M et al (2020) Model of effective width and fracture conductivity for hydraulic fractures in tight reservoirs. *Arab J Sci Eng* 45(9):7821–7834
- Katende A, Allen C, Massion C, et al (2022) Experiments and Modeling of Proppant Embedment and Fracture Conductivity for the Caney Shale. ARMA-2022–0805, Oklahoma, USA. In: 56th US Rock Mechanics/Geomechanics Symposium
- Katende A, O'Connell L, Rich A et al (2021a) A comprehensive review of proppant embedment in shale reservoirs: experimentation, modeling and future prospects. *J Nat Gas Sci Eng* 95:104143
- Katende A, Rutqvist J, Bengte M et al (2021b) Convergence of micro-geochemistry and micro-geomechanics towards understanding proppant shale rock interaction: a Caney shale case study in southern Oklahoma, USA. *J Nat Gas Sci Eng* 96:104296
- Kong D, Gao J, Lian P et al (2022a) Characteristics of gas-oil contact and mobilization limit during gas-assisted gravity drainage process. *Adv Geo-Energy Res* 6(2):169–176
- Kong D, Gao J, Zhu W et al (2022b) Experimental study on conductivity and stress sensitivity of fully supported fractured shale cores. *J Pet Sci Eng* 218:110971
- Kong D, Li Y, Sarma H et al (2019) Investigation into micro-physico-chemical interaction between sodium dodecylbenzene sulfonate (SDBS) and partially hydrolyzed polyacrylamide (HPAM) utilizing electron probe microanalysis method. *Colloids Surf A* 561:187–193
- Li H, Zhu W, Niu H et al (2022) 2-D porous flow field reveals different EOR mechanisms between the biopolymer and chemical polymer. *J Pet Sci Eng* 210:110084
- Liang X, Zhou F, Liang T et al (2020) The effect of combined proppants upon the fracture conductivity in tight gas reservoirs. *Energy Rep* 6:879–884
- Liew MS, Danyaro KU, Zawawi NAWA (2020) A comprehensive guide to different fracturing technologies: a review. *Energies* 13:3326
- Liu S, Dou X, Zeng Q, Liu J (2021a) Critical parameters of the Jamin effect in a capillary tube with a contracted cross section. *J Pet Sci Eng* 196:107635
- Liu S, Huang J, Tang S et al (2020a) Experimental study on the damage of artificial fracture permeability in coal during the flow back of guar-based fracturing fluid. *Geofluids* 2020:1–13
- Liu W (2020) Exact analytical solutions of non-Darcy seepage flow problems of one-dimensional Bingham fluid flow in finite long porous media with threshold pressure gradient. *J Pet Sci Eng* 184:106475
- Liu X, Kang Y, Li J et al (2020b) Percolation characteristics and fluid movability analysis in tight sandstone oil reservoirs. *ACS Omega* 5:14316–14323
- Liu Y, Mu S, Guo J et al (2021b) Model for fracture conductivity considering particle size distribution in a proppant monolayer. *J Nat Gas Sci Eng* 95:104188
- Melcher H, Mayerhofer M, Agarwal K, et al. (2020) Shale frac designs move to just-good-enough proppant economics. SPE-199751-MS, In: SPE Hydraulic Fracturing Technology Conference and Exhibition
- Muther T, Qureshi HA, Syed FI et al (2021) Unconventional hydrocarbon resources: geological statistics, petrophysical characterization, and field development strategies. *J Pet Explor Prod Technol* 12:1463–1488
- Ni X, Niu Y, Wang Y, Yu K (2018) Non-Darcy flow experiments of water seepage through rough-walled rock fractures. *Geofluids* 2018:8541421
- Ostad-Ali-Askari K, Ghorbanizadeh Kharazi H, Shayannejad M, Zareian MJ (2019) Effect of management strategies on reducing negative impacts of climate change on water resources of the Isfahan-Borkhar aquifer using MODFLOW. *River Res Appl* 35:611–631
- Qiao J, Zeng J, Jiang S et al (2022) Investigation on the unsteady-state two-phase fluid transport in the nano-pore system of natural tight porous media. *J Hydrol* 607:127516
- Shen P-F, Li G, Li X-S et al (2021) Application of fracturing technology to increase gas production in low-permeability hydrate reservoir: a numerical study. *Chin J Chem Eng* 34:267–277
- Syed FI, Muther T, Van VP et al (2022) Numerical trend analysis for factors affecting EOR performance and CO<sub>2</sub> storage in tight oil reservoirs. *Fuel* 316:123370
- Voltolini M, Ajo-Franklin J (2020) Evolution of propped fractures in shales: the microscale controlling factors as revealed by in situ X-Ray microtomography. *J Pet Sci Eng* 188:106861
- Wang R, Yang J, Wang M et al (2019) Effect of threshold pressure gradients on control areas determination of production well in CBM reservoirs. *Adv Polym Technol* 2019:1–10
- Wu Y, Pan Z, Zhang D et al (2018) Experimental study of permeability behaviour for proppant supported coal fracture. *J Nat Gas Sci Eng* 51:18–26
- Wu Z, Cui C, Jia P et al (2021) Advances and challenges in hydraulic fracturing of tight reservoirs: a critical review. *Energy Geosci* 3:427–435
- Wu Z, Cui C, Trivedi J et al (2019) Pressure analysis for volume fracturing vertical well considering low-velocity non-Darcy flow and stress sensitivity. *Geofluids* 2019:1–10
- Xiao H, Li Z, He S et al (2021a) Experimental study on proppant diversion transportation and multi-size proppant distribution in complex fracture networks. *J Pet Sci Eng* 196:107800
- Xiao J, Song F, Jiang J, et al. (2021) Threshold pressure experiment of liquid flows through nano-channels and tight cores. *J Phys: Conf Ser* 2076:012028.
- Xu J, Ding Y, Yang L et al (2021) Conductivity analysis of tortuous fractures filled with non-spherical proppants. *J Pet Sci Eng* 198:108235
- Xu J, Ding Y, Yang L et al (2019) Effect of proppant deformation and embedment on fracture conductivity after fracturing fluid loss. *J Nat Gas Sci Eng* 71:102986
- Ye W, Wang X, Cao C, Yu W (2019) A fractal model for threshold pressure gradient of tight oil reservoirs. *J Pet Sci Eng* 179:427–431

- You L, Xie B, Yang J et al (2019) Mechanism of fracture damage induced by fracturing fluid flowback in shale gas reservoirs. *Nat Gas Ind B* 6:366–373
- Zhang R, Hou B, Tan P et al (2020) Hydraulic fracture propagation behavior and diversion characteristic in shale formation by temporary plugging fracturing. *J Pet Sci Eng* 190:107063
- Zhang W, Zhao Q, Guan X et al (2022) Experiment and model of conductivity loss of fracture due to fine-grained particle migration and proppant embedment. *Energies* 15:2359
- Zhao L, Jiang H, Wang H et al (2020a) Representation of a new physics-based non-Darcy equation for low-velocity flow in tight reservoirs. *J Pet Sci Eng* 184:106518
- Zhao M, Li Y, Xu Z et al (2020b) Dynamic cross-linking mechanism of acid gel fracturing fluid. *Colloids Surf A* 607:125471
- Zhao Z, He J, Guo J et al (2022) Study on proppant embedment in rough fracture surface based on three dimension laser scanning. *J Pet Sci Eng* 219:111077
- Zheng W, Liu Y, Liu Y et al (2019) Experimental study on fluid flow in micro-fractures contained within matrix. *Arab J Geosci* 12:1–9
- Zheng W, Silva SC, Tannant DD (2018) Crushing characteristics of four different proppants and implications for fracture conductivity. *J Nat Gas Sci Eng* 53:125–138
- Zhi S, Elsworth D (2020) Proppant embedment in coal and shale: impacts of stress hardening and sorption. *Int J Coal Geol* 227:103545
- Zhu W, Liu Y, Shi Y et al (2022) Effect of dynamic threshold pressure gradient on production performance in water-bearing tight gas reservoir. *Adv Geo-Energy Res* 6(4):286–295

**Publisher's Note** Springer Nature remains neutral with regard to jurisdictional claims in published maps and institutional affiliations.